

Integration of 555 temperature sensors into a 64 × 192 CMOS image sensor

Abarca, Accel; Xie, Shuang; Markenhof, Jules; Theuwissen, Albert

DOI

[10.1016/j.sna.2018.09.029](https://doi.org/10.1016/j.sna.2018.09.029)

Publication date

2018

Document Version

Accepted author manuscript

Published in

Sensors and Actuators, A: Physical

Citation (APA)

Abarca, A., Xie, S., Markenhof, J., & Theuwissen, A. (2018). Integration of 555 temperature sensors into a 64 × 192 CMOS image sensor. *Sensors and Actuators, A: Physical*, 282, 243-250.
<https://doi.org/10.1016/j.sna.2018.09.029>

Important note

To cite this publication, please use the final published version (if applicable).
Please check the document version above.

Copyright

Other than for strictly personal use, it is not permitted to download, forward or distribute the text or part of it, without the consent of the author(s) and/or copyright holder(s), unless the work is under an open content license such as Creative Commons.

Takedown policy

Please contact us and provide details if you believe this document breaches copyrights.
We will remove access to the work immediately and investigate your claim.

Integration of 555 Temperature Sensors into a 64 × 192 CMOS Image Sensor

Authors

Accel Abarca¹, Shuang Xie¹, Jules Markenhof^{1,2} and Albert Theuwissen^{1,3}

1 Electronic Instrumentation Laboratory, TU Delft, 2628 CD, Delft, The Netherlands

2 now with Texas Instruments, 5656 AE, Eindhoven, The Netherlands

3 Harvest Imaging, 3960, Bree, Belgium

a.n.abarcaprouza@tudelft.nl; +31-15-27-86432

s.xie@tudelft.nl

j-markenhof@ti.com

albert@harvestimaging.com

Abstract

In this work, a novel approach for measuring relative temperature variations across the active area of a CMOS image sensor itself is presented. 555 Image pixels have been replaced by temperature sensors pixels (Tixels) in the same pixel array layer. Both sensors, pixels and Tixels, utilize the same readout structure to obtain the data. This approach of measuring temperature variations in the pixel array can be used to compensate for dark signal non-uniformity. Measurements of dark current and temperature have been performed in a temperature range of -40 and 90 °C. Results show that pixels and Tixels are working by using the same readout system based on source followers and column amplifiers. The average dark current of the image sensor increases with temperature in the temperature range of -40 and 60 °C, and at the same time, Tixels show high linear response, having a temperature error less than 0.6 °C after a 1st order best curve fitting.

1 Introduction

One of the major contributors of fixed pattern noise (FPN) in image sensors is the dark current or leakage current. It highly depends on process variations and temperature variations. It has been reported that dark current doubles its value every 5-6 °C for temperatures above 10 °C [1,2]. Dark current can be compensated by means of a dark reference frame. To grab a dark reference frame a mechanical global shutter is needed. However, in the case of mobile phones the mechanical shutter is not available. Also, efforts to reduce the effect of dark current has been made by modifying the photodetector at physical level. Some of these techniques are: adding a p-well layer surrounding the pixel [3], or by using a buried-channel source follower instead of a surface-mode source follower [4]. This work proposes to integrate temperature sensors in the same layer as the image pixels and using the same readout system to obtain the data of the pixel-Tixel sensors. In this way, relative temperature variations can be measured as well as temperature distribution along the pixel array. This temperature data can give important information to compensate for dark current after calibration of the Tixels and pixels in terms of the dark current for different temperatures. For instance, it could be possible to recreate a dark reference frame by using the temperature measurements of the Tixels.

In the following sections the architecture of the sensors will be explained as well as the measurement setup. Then measurement results will be presented finalizing with conclusions.

2 Description of the Sensor

The sensor array is composed of image pixels and temperature sensor pixels. In the following subsections both sensors will be presented.

2.1 Pixel Architecture

The image pixels are based on a typical CMOS 4T (4 transistors) architecture. This architecture is composed of 4 transistors: the reset transistor (RST), the transfer gate (TG) + pinned photodiode (PPD) + floating diffusion (FD), and two transistors constitute the nMOS source follower and select transistor (RS). In this architecture, the incoming light is collected by the pinned photodiode as electrical charge while the transfer gate is closed. When the TG is open, all this charge is transferred to the floating diffusion where the charge is converted into voltage signal. Then, this signal is read by using the source follower before to be amplified by the column amplifier block. The 4T architecture allows full noiseless charge transfer due to the pinned photodiode configuration. The diode is fully depleted when the diode is exposed to a voltage higher (or equal) than the pinning voltage while the TG is on [5,6]. Other features of the 4T architecture are: low noise, low dark current and high quantum efficiency [7].

In this work, the size of the image pixel is 11 μm by 11 μm . The test array is composed of 64 rows and 192 columns which means having 11733 image pixels in total (excluding the Tixels). The schematic of the 4T pixel is shown in Figure 1 (a).

2.2 Tixel Architecture

On the other hand, the Tixel is composed of a parasitic Bipolar Junction Transistor (BJT), which is the core of the Tixel, a column selector and a pMOS source follower, as shown in Figure 1 (b). In this case, a pMOS source follower has been used instead of an nMOS source follower as in the case of the pixels. The reason is that, the pMOS source follower exhibits better linearity in the Tixel signal output range compare to the nMOS based one. In terms of temperature sensors, BJT based temperature sensor exhibits better accuracy, lower process variations and fast measurement, compared to a CMOS alternative [8,9]. The temperature is obtained via the differential base-emitter voltage (ΔV_{BE}) which is proportional to the absolute temperature (PTAT) [10], as equation (1) shows.

$$\Delta V_{BE} = \frac{kT}{q} \ln(r) \rightarrow T = \frac{\Delta V_{BE} q}{k \ln(r)} \quad (1)$$

Where k corresponds to the Boltzmann constant, T is the absolute temperature, r is the ratio between two different biasing currents, and q corresponds to the electric charge. To obtain the ΔV_{BE} , the BJT is biased by two different currents in a ratio 4:1 (thus $r = 4$). These currents are generated by an internal current mirror block which is biased by an external 1 μA current.

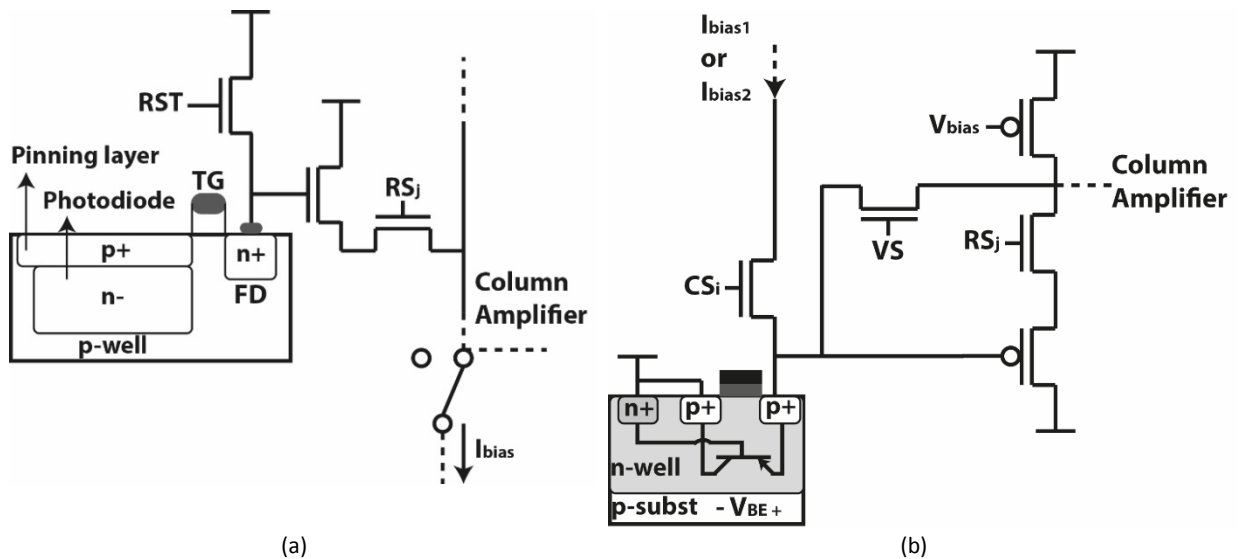


Figure 1. (a) 4T image pixel architecture; (b) Tixel architecture based on BJT.

The Tixel is selected (and turned on) by a column decoder that controls the CS_i transistor. When this transistor is on, then the BJT can be biased by the two different currents (ratio 4:1). The base-emitter signal is then read by the pMOS source follower before being amplified by the column amplifier. There are two operation modes to obtain the data of the Tixel, these are shown in Figure 2.

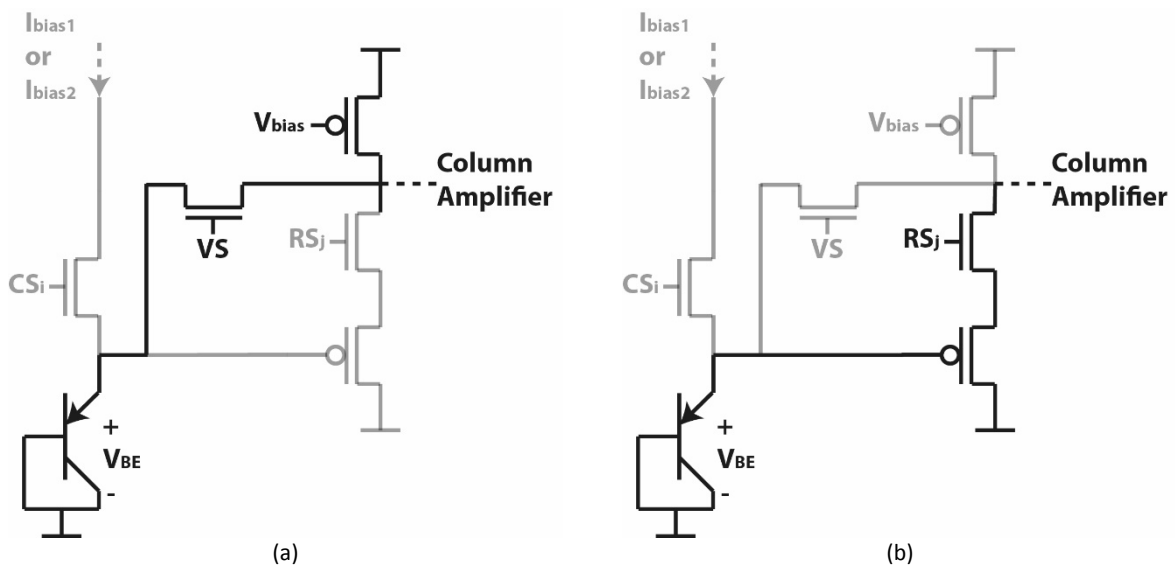


Figure 2. (a) Direct mode; (b) Indirect mode.

The first operation mode corresponds to the direct mode. In this case, the ΔV_{BE} signal (temperature) is read via the VS transistor, as shown in Figure 2 (a). Direct mode only allows reading the Tixels (excluding the pixels). The second operation mode corresponds to the indirect mode. The temperature signal is obtained via the RS_j transistor, as shown in Figure 2 (b). This transistor is also present in the pixel (Figure 1(a)), and it is controlled by the same control signal allowing that both, the pixels and the Tixels, can be read in the same readout cycle.

The size of the Tixel is 11 μm by 22 μm , thus twice the size of a pixel. The size of the Tixel is bigger than the pixel because of the extra transistors of the Tixels that are used in the direct and indirect mode. 555 Tixels have been uniformly integrated in the same layer as the pixels, having approximately 3 Tixels per row and 8 Tixels per column.

The test chips have been fabricated by a standard 0.18 μm CMOS Image Sensor (CIS) TowerJazz Technology.

3 Readout System

The same control signals and readout structure are used by pixels and Tixels. The readout system is composed of Row and Column decoders. These decoders generate the signals to select each position in the image array. It is also used to select the source followers and the column amplifiers.

There is a biasing block that provides the bias currents to the Tixels. It generates three different ratios 4:1, 3:1, and 2:1. The output signals of the pixels or Tixels are amplified by the column amplifier block. This block is composed of a Programmable Gain Amplifier (PGA) and the Correlated Doubling Sampling (CDS) circuit. The PGA provides 5 different gains: 1, 2, 4, 8, and 16. The CDS circuit is used to cancel the kTC noise of the image sensor [11,12]. Then, the amplified signal ($A \cdot \Delta V_{BE}$) is buffered by an output buffer circuit before to be digitalized by an off-chip 16 bits ADC [13]. The block diagram of the readout system is presented in Figure 3.

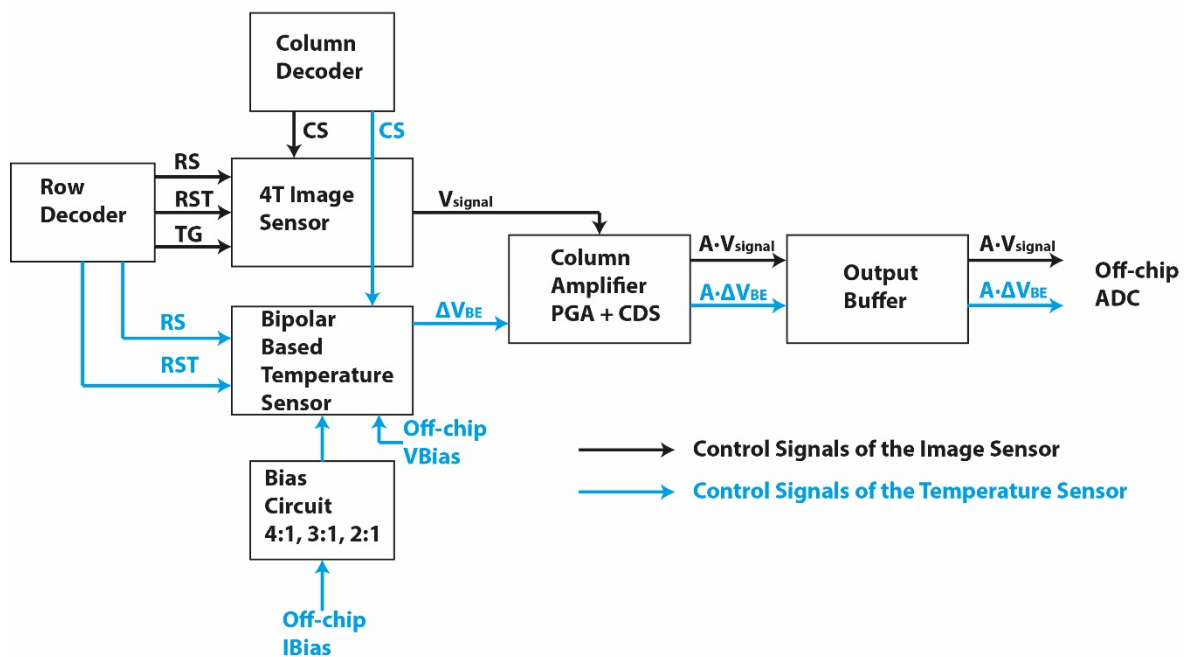


Figure 3. Block diagram of the readout system.

4 Measurement Setup

The measurement setup is composed of a PCB, FPGA, a PC with Quartus and LabView, and a temperature controlled oven. The chip is mounted on the PCB that provides all the power supplies of the chip and it also contains the 16 bits ADC. The FPGA generates all the control signals for the chip and for the ADC. The FPGA is configured by using Quartus. The data of the chip is grabbed by utilizing LabView. Two different temperature controlled ovens have been used depending on the temperature range. For the temperature range between 20 and 90 $^{\circ}\text{C}$ a Binder FP53 oven was used. On the other hand, for the temperature range between -40 and 90 $^{\circ}\text{C}$ a Vötsch VT7004 oven was used.

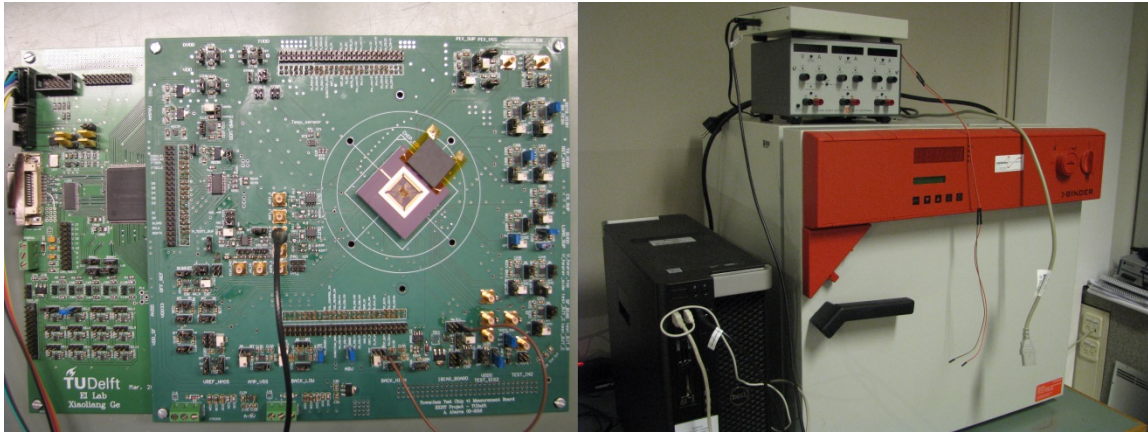


Figure 4. Measurement setup.

5 Measurement results

A micro-photograph of the chip has been taken, as shown in Figure 5. The Figure shows the different circuit blocks of the chip. The image sensor is placed in the top middle part of the picture. Here it is possible to see the presence of the TixelS along the array (in light orange). Below the image sensor, the column amplifier and the output buffer are presented. Row and column decoders are placed to the left of the image sensor.

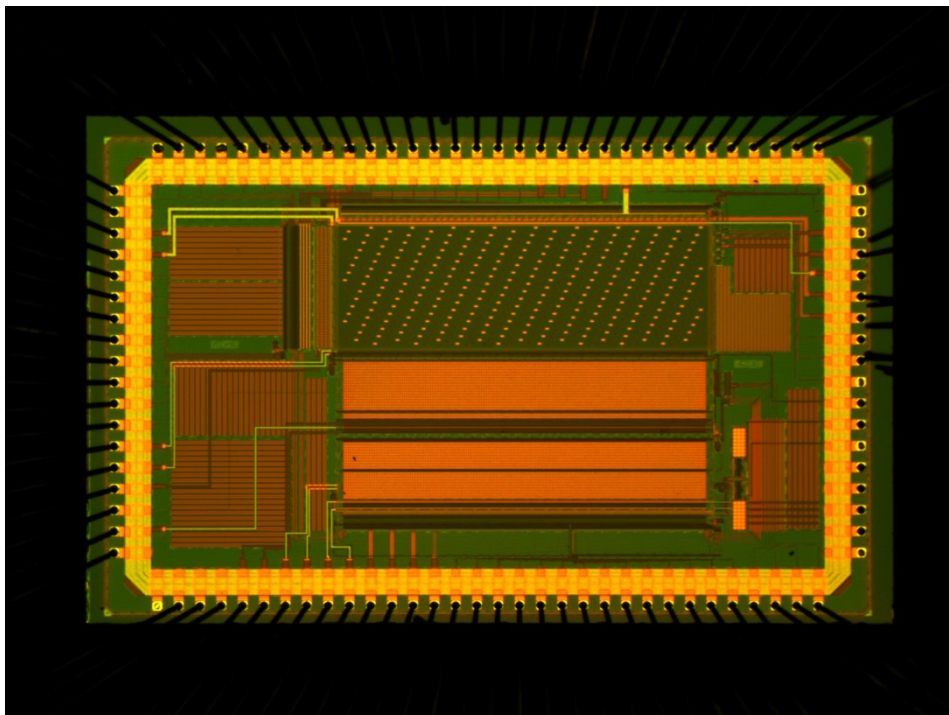


Figure 5. Micro-photograph of the chip.

5.1 Image Sensor

A photo has been taken by using the image sensor, as shown in Figure 6. The black dots prove the presence of the temperature sensors along the array. This picture basically confirms that the image sensor as well as the readout system is working.

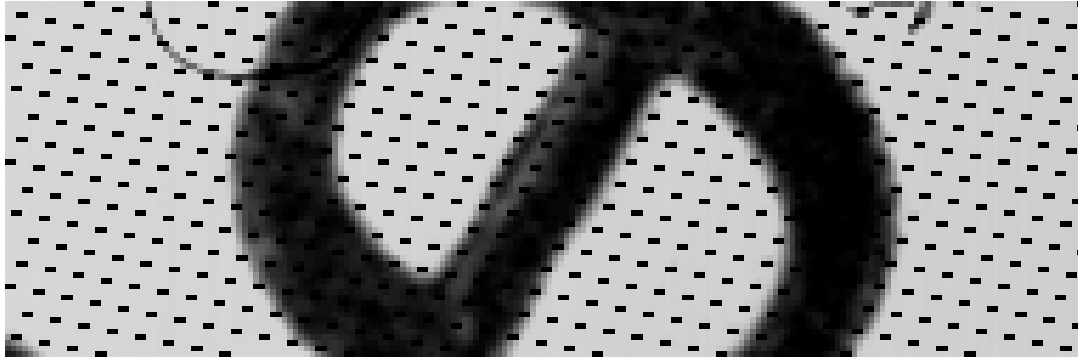


Figure 6. Photo taken by the image sensor.

One parameter that has been measured is the conversion gain. It has been calculated averaging 100 frames and all the pixels (excluding the Tixels). This measurement was done at room temperature (RT) by using a constant exposure light. The value of the conversion gain is $71.57 \mu\text{V}/e^-$, and it is used to calculate the dark current of the image sensor in terms of electrons (e^-).

The dark current has been measured in time and in temperature. The dark current has been calculated averaging 100 frames and 10000 pixels. It was obtained at 30°C in the exposure time range of 0.05 s and 5 s. Figure 7 (a) shows the average dark signal vs. time. The dark current exhibits the expected linear behaviour having a value of $119.9 e^-/s$ @ 30°C .

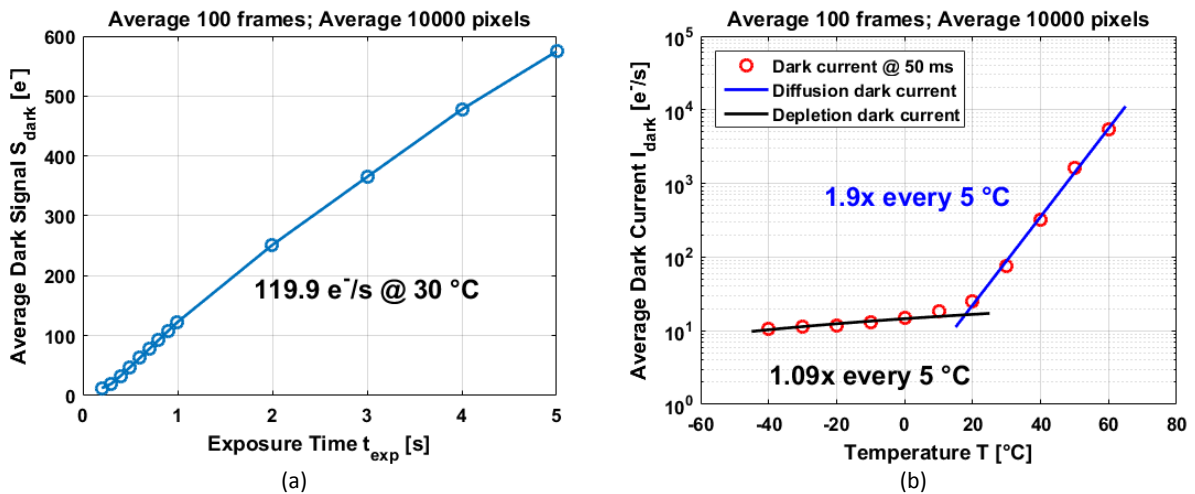


Figure 7. (a) Dark signal vs. time. (b) Dark current vs. temperature.

The dark current has been also measured in a temperature range of -40 and 60°C @ 50 ms exposure time. Averaging 100 frames and 10000 pixels, the average dark current exhibits two different curves, as shown in Figure 7 (b). Both curves increase exponentially but in a different rate depending on the temperature range. Between -40 and 10°C , the dark current increases 1.09 times every 5°C while in the range of 20 and 60°C the dark current increases 1.9 times every 5°C .

In most cases, two dominant dark current mechanisms are considered: at low temperatures the depletion dark current dominates [14,15] and at high temperatures diffusion dark current is the dominant mechanism [15,16]. In both mechanisms, the dark current has an exponential behaviour increasing ~ 1.5 times every 5°C at low temperatures, while at high temperatures the dark current increases ~ 2 times every 5°C [14,16,17]. At temperatures higher than 10°C , the pixel-Tixel sensor shows a behaviour where the diffusion dark current dominates. However, at low temperatures it seems the depletion dark current is not the only (or the dominant) mechanisms involved because the

increment is only 1.09 times per 5 °C instead of ~1.5 times per 5 °C. Also, if the dark current is extrapolated for low temperatures, the values are considerably lower in magnitude as compared to the measured values. The cause of the higher dark current values and the lower increment in temperature might be due to two different effects: It has been observed that during measurements in dark (between -40 and 60 °C), pixels next to Tixels have a higher output signal compared to those farthest from the Tixels, as shown in Figure 8 (a). A similar effect has been reported when BJTs or diodes are next to the image array generating charge that causes an increment in the output signal of the pixels [18,19]. Additionally, the voltage dependency of the dark current on the level of the floating diffusion has been measured at -20 °C and at four different voltage levels: 2.5 V, 2.8 V, 3.0 V, and 3.3 V. Figure 8 (b) shows the voltage dependency of the dark signal, increasing when the voltage level increases. This could point to the presence of tunnelling current on the floating diffusion level. These two effects might add extra signal to the depletion dark current at low temperatures, obtaining higher levels of dark current and an increment of only 9% every 5 °C (Figure 7 (b)).

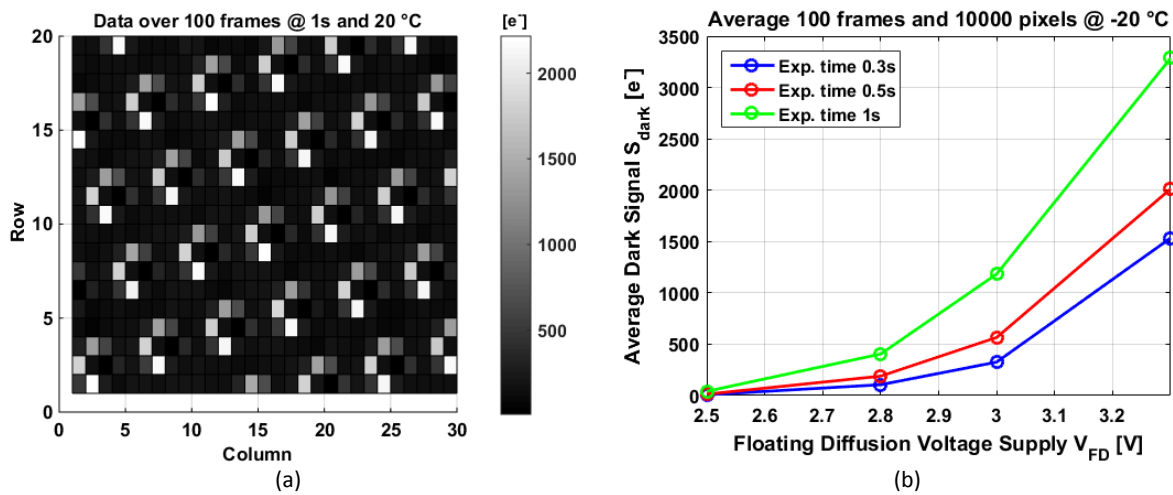


Figure 8. (a) Presence of hot pixels next to the Tixels. (b) Dark current dependency on the level of the FD voltage supply.

5.2 Temperature Sensor

Temperature measurements have been done by using two different temperature control ovens: Binder FP53 in a temperature range of RT and 90 °C; and Vötsch model VT7004 in a temperature range of -40 and 90 °C. In both cases the chip has been placed on top of a massive aluminium block to stabilize the temperature reaching an accuracy of 0.015 °C. As a reference the temperature of the chip-Al block has been measured/controlled by a calibrated PT100 thermistor (for both ovens to avoid duplicity of the temperature data). Two different gains of the on-chip PGA have been used: Gain 16 (G16) and Gain 8 (G8). 4 different chips have been tested (C1, C2, C3, and C4).

All Tixels of chip sample C1 have been plotted between RT and 90 °C in Figure 9 (a). Figure 9 (a) shows that the output signal (V_{out}) of all Tixels is linear between RT and 90 °C. The V_{out} -temperature coefficient of the Tixels is in between 1.2045 mV/°C and 1.2104 mV/°C. In this case, the coefficient deviation is 0.7% from the average value. All Tixels measure almost the same relative temperature variation. This means that it would be possible to measure temperature variations with any Tixel in the pixel array.

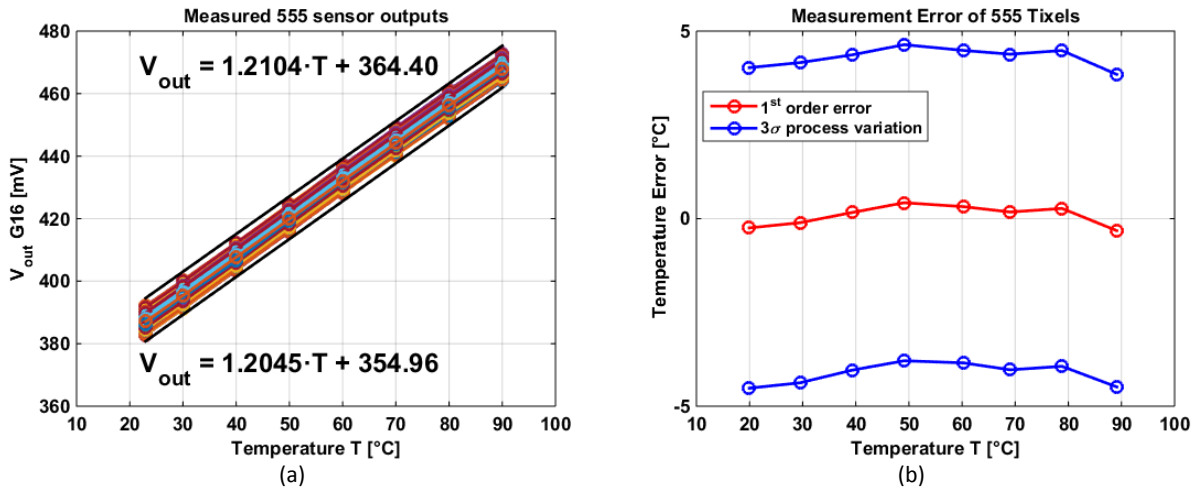


Figure 9. (a) Temperature behaviour of the 555 Tixels of chip C1 using G16. (b) Process variations of chip C1.

The Tixels process variation of C1 shows a relatively high 3σ standard deviation of ± 4 °C, as shown in Figure 9 (b).

On the other hand, 4 different chips have been measured between RT and 90 °C by using G16 and G8. In the case of G16, and averaging 555 Tixels, the 4 chips show a high linearity in this temperature range (Figure 10 (a)). The temperature coefficient of all chips has an average value of 1.2186 mV/°C with a deviation of 0.8% from the average coefficient. The temperature error has been calculated by using a 1st order best curve fitting (Figure 10 (b)).

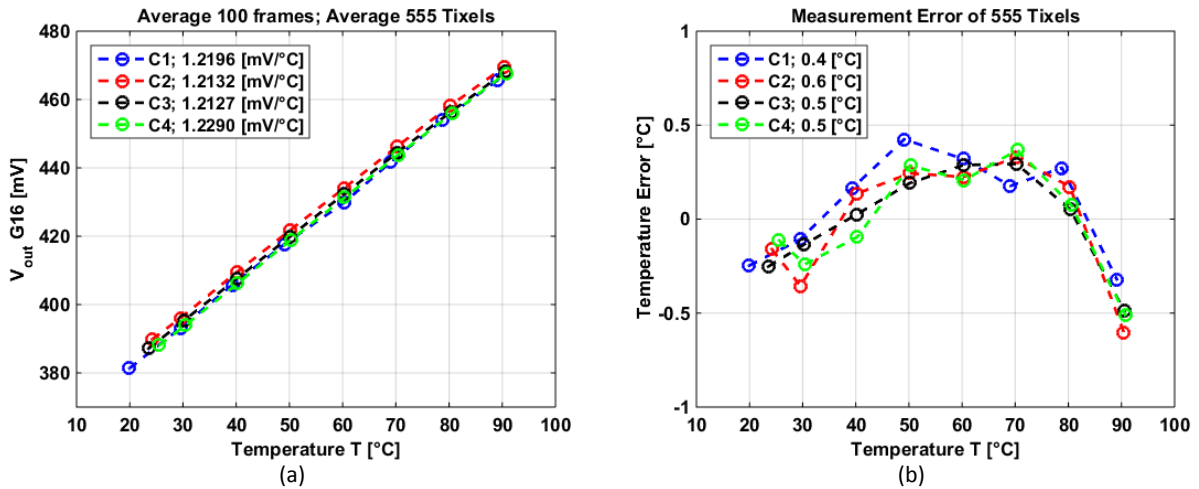


Figure 10. (a) Temperature behaviour of 4 chips averaging 100 frames and 555 Tixels using gain of 16. (b) Temperature error after 1st order best curve fitting.

The temperature error of the 4 chips shows a similar behaviour, having a maximum error of 0.6 °C for chip C2.

The same measurements have been done but using G8. In this case, the V_{out} -temperature curve exhibits high linearity as well as in the case of G16 (Figure 11 (a)). The average temperature coefficient of the 4 chips has a value of 0.6576 mV/°C with a deviation of 2% from the average.

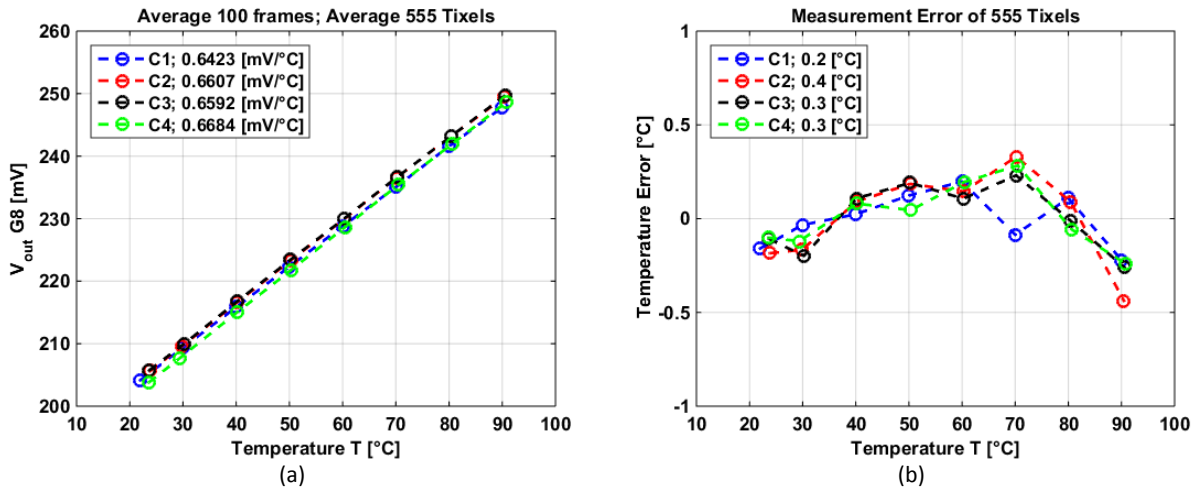


Figure 11. (a) Temperature behaviour of 4 chips averaging 100 frames and 555 Tixels using gain of 8. (b) Temperature error after 1st order best curve fitting.

The maximum error after 1st order best curve fitting is 0.4 °C for chip C2.

Chip C1 has been measured in a larger temperature range between -40 and 90 °C. Averaging 100 frames and all the Tixels, the V_{out} -temperature curve presents a 2nd order behaviour, as shown in Figure 12 (a). This measurement error corresponds to 1.4% of curvature.

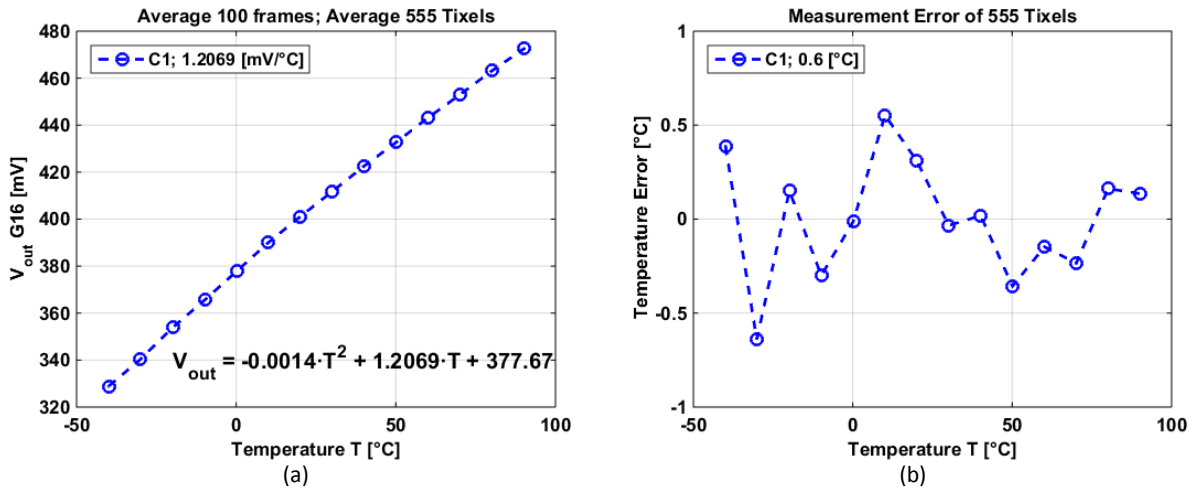


Figure 12. (a) Temperature behaviour of chip C1 averaging 100 frames and 555 Tixels using gain of 16 in a temperature range of -40 and 90 °C. (b) Temperature error after 2nd order best curve fitting.

After a 2nd order best curve fitting, the temperature error shows more variation at low temperatures [-40 to 10] °C than at high temperatures [20 to 90] °C where the maximum error is 0.6 °C.

The main characteristics of the Tixel are shown in Table 1.

Table 1. Characteristics of the Tixel from 20 to 90 °C.

| | |
|-----------------------|-------------------------------|
| Resolution | 0.025 °C |
| Accuracy | ±0.6 °C @ G16 ±0.4 °C @ G8 |
| Conversion Time | 0.5 ms |
| Area | 11 µm x 22 µm |
| Technology | 0.18 µm |
| Supply | 3.3 V |
| Current | 1 – 4 µA |
| Energy per Conversion | 4.1 nJ |

6 Conclusions

Temperature sensors have been integrated in an image array having 555 Tixels uniformly distributed along the array. Tixels are based on parasitic BJTs. Results have shown that both sensors are working by using the same readout system as well as the same control signals to grab the data of the regular pixels. The image sensor has a dark current of 119.9 e⁻/s @ 30 °C. The dark current of the image sensor increases 1.09 times every 5 °C in the temperature range of -40 and 10 °C and 1.9 times every 5 °C in the range of 20 and 60 °C. The dark current behaviour at low temperatures seems to have other mechanisms involved (not only due to depletion dark current) as measurements have shown. These other mechanisms might be charge generated in the Tixels and tunnelling current on the floating diffusion. These two effects could add extra signal to the dark current at low temperatures. On the other hand, the dark current behaviour at high temperatures is associated to diffusion dark current.

The Tixels show high linearity between RT and 90 °C, individually and averaging all of them. Individually, every Tixel can measure almost the same relative temperature variations along the array because they have a coefficient deviation of 0.7% from the average. However, the Tixels exhibit a relatively high process variations, thus it would not be possible to measure thermal gradients along the array. In the case of G16, the conversion coefficient is close to 1.2186 mV/°C and a maximum error of 0.6 °C after a 1st order best curve fitting. Using G8, the conversion coefficient is close to 0.6576 mV/°C with an error of 0.4 °C. When measuring in a larger temperature range of -40 and 90 °C, averaging all Tixels of chip C1, the output signal exhibits a 2nd order measurement error with a conversion coefficient of 1.2069 mV/°C. The error in this case is 0.6 °C.

These results have shown that the dark current can be compensated by using the measurements of the Tixels because, on the one hand, the dark current of this image sensor is temperature dependent, and at the same time, it is possible to measure temperature by using the Tixels.

In the future, different kind of Tixels, like based on CMOS, will be explored to integrate in the pixel array as well as reducing the size of the Tixel to only one pixel area. Different readout systems will be explored as well.

Acknowledgements

The authors acknowledge TowerJazz for the prototypes CIS devices. The research is part of the CISTERN project (a European ECSEL Joint Undertaken project), funded by the Dutch Government.

References

1. X. Wang, Noise in Sub-Micron CMOS Image Sensors. PhD Dissertation, Delft University of Technology, Delft, the Netherlands, 3rd November 2008, pp. 46-68. [uuiid:2f31c7c5-5019-4cab-a9c5-65528f886a76](https://doi.org/10.1109/2f31c7c5-5019-4cab-a9c5-65528f886a76)
2. P.S. Baranov, V.T. Litvin, D.A. Belous, A.A. Mantsvetov, Dark Current of the Solid-State Imagers at High Temperature. EIconRus IEEE Conference of Russian, Saint Petersburg, Russia, 1-3 February 2017; pp. 635-638. DOI: [10.1109/EIconRus.2017.7910636](https://doi.org/10.1109/EIconRus.2017.7910636)
3. S.-W. Han, E. Yoon, Low Dark Current CMOS Image Sensor Pixel with Photodiode Structure Enclosed by P-well. Electronics Letters, vol. 42, no. 20, pp. 1145-1146, 9th October 2006. DOI: [10.1049/el:20061652](https://doi.org/10.1049/el:20061652)
4. X. Wang, M.F. Snoeij, P.R. Rao, A. Mierop, A.J. Theuwissen, A CMOS Image Sensor with a Buried-Channel Source Follower. 2008 IEEE ISSCC – Digest of Technical Papers, pp. 62-63 (595), 9th January 2009. DOI: [10.1109/ISSCC.2008.4523057](https://doi.org/10.1109/ISSCC.2008.4523057)
5. R. Coath, J. Crooks, A. Godbeer, M. Wilson, R. Turchetta, Advanced Pixel Architectures for Scientific Image Sensors. Topical Workshop on Electronics for Particle Physics, Paris, France, 21-25 September 2009; pp. 57-61.
6. A. Godbeer, Investigation of 4T CMOS Image Sensor Design and the Effects of Radiation Damage. MPhys Dissertation, University of Surrey, Guildford, United Kingdom, 12th February 2010, pp. 14-15. <http://epp.fnal.gov/DocDB/0016/001648/001/Adam-Godbeer.pdf>
7. E.R. Fossum, D.B. Hondongwa, A Review of the Pinned Photodiode for CCD and CMOS Image Sensors. IEEE J. Electron Devices Soc. 2014, vol. 2, no. 3, pp. 33-43. DOI: [10.1109/JEDS.2014.2306412](https://doi.org/10.1109/JEDS.2014.2306412)
8. K. Souri, Y. Chae, K. Makinwa, A CMOS Temperature Sensor with a Voltage-Calibrated Inaccuracy of ± 0.15 °C (3σ) from -55 °C to 125 °C. IEEE Journal of Solid-State Circuits 2013, vol. 48, no.1, pp. 292-301. DOI: [10.1109/JSSC.2012.2214831](https://doi.org/10.1109/JSSC.2012.2214831)
9. G.C. Meijer, G. Wang, F. Fruett, Temperature Sensors and Voltage References Implemented in CMOS Technology, IEEE Sensors Journal 2001, vol. 1, no. 3, pp. 225-234. DOI: [10.1109/JSEN.2001.954835](https://doi.org/10.1109/JSEN.2001.954835)
10. M.A.P. Pertijs, K.A.A. Makinwa, J.H. Huijsing, A CMOS Smart Temperature Sensor with a 3σ Inaccuracy of ± 0.1 °C from -55 °C to 125 °C. IEEE Journal of Solid-State Circuits, vol. 40, no. 12, December 2005, pp. 2805-2815. DOI: [10.1109/JSSC.2005.858476](https://doi.org/10.1109/JSSC.2005.858476)
11. J. Tan, 4T CMOS Active Pixel Sensors under Ionizing Radiation. PhD Dissertation, Delft University of Technology, Delft, the Netherlands, 15th April 2013, pp.28-29. DOI: [10.4233/uuiid:12cb7563-45db-4824-bcf7-8f5af11ff52f](https://doi.org/10.4233/uuiid:12cb7563-45db-4824-bcf7-8f5af11ff52f)
12. S.K. Mendis, S. Kemeny, R.C. Gee, B. Pain, C.O. Staller, Q. Kim, CMOS Active Pixel Image Sensors for Highly Integrated Imaging Systems. IEEE Journal of Solid-State Circuits, vol. 32, no. 2, February 1997, pp. 187-197. DOI: [10.1109/4.551910](https://doi.org/10.1109/4.551910)
13. <http://www.analog.com/media/en/technical-documentation/data-sheets/AD9826.pdf>
14. R. Widenhorn, M.M. Blouke, A. Weber, A. Rest, E. Bodegom, Temperature Dependence of Dark Current in a CCD. Proc. SPIE 4669 Sensors and Camera Systems for Scientific, Industrial, and Digital Photography Applications III, 1st April 2002, pp. 193-201. DOI: [10.1117/12.463446](https://doi.org/10.1117/12.463446).
15. W.C. Porter, B. Kopp, J.C. Dunlap, R. Widenhorn, E. Bodegom, Dark Current Measurements in a CMOS Imager. Proc. SPIE 6816 Sensors, Cameras, and Systems for Industrial/Scientific Applications IX, 29th February 2008, pp. 1-8. DOI: [10.1117/12.769079](https://doi.org/10.1117/12.769079)
16. K. Yasutomi, Y. Sadanaga, T. Takasawa, S. Itoh, S. Kawahito, Dark Current Characterization of CMOS Global Shutter Pixels Using Pinned Storage Diodes. Proc. of International Image Sensor Workshop, 8-11 June 2011.
17. H.I. Kwon, I.M. Kang, B-G. Park, J.D. Lee, S.S. Park, The Analysis of Dark Signals in the CMOS APS Imagers from the Characterization of Test Structures. IEEE Transactions on Electron Devices, vol. 51, no. 2, February 2004, pp. 178-184. DOI: [10.1109/TED.2003.821765](https://doi.org/10.1109/TED.2003.821765)
18. G. Meynants, W. Diels, J. Bogaerts, W. Ogiers, Emission Microscopy Analysis of Hot Cluster Defects of Imagers Processed on SOI. 2013 International Image Sensor Workshop, USA, June 2013.
19. K. Seo, S. Lee, P. Ahn, D. Kim, K. Cho, A Study on Photon Effect to Image Plane. 2017 International Image Sensor Workshop, Japan, May-June 2017.